ORIGINAL PAPER

Mapping snow cover using landsat data: toward a fine-resolution water-resistant snow index

Cenk Donmez[1] · Suha Berberoglu[1] · Sevim Yasemin Cicekli[2] · Ahmet Cilek[1] · Ali Nadir Arslan[3]

Abstract

Snow cover is of significant importance to freshwater supplies and influences the hydrology of different altitudes in mountainous regions. The monitoring of snow cover over the Mediterranean region of Turkey is of high priority due to its rapid irregularities experienced during the past decades. These irregularities in snow cover might especially lead to severe risks for the local ecosystems, such as rivers, and irrigated agriculture. Water-Resistant Snow Index (WSI) is a new and powerful spectral index for mapping snow cover using Moderate Resolution Imaging Spectroradiometer (MODIS) data. There still exists a large knowledge gap about how to improve the finer resolution applications of WSI. This study aimed to explore the applicability of WSI using Landsat TM and OLI images with a better spatial resolution to a complex catchment in the eastern Mediterranean region of Turkey. The WSI maps derived from both MODIS/Terra-MOD09A1 and Landsat images from 2005 to 2018 were compared with the high-resolution Sentinel-2A data. The comparative analysis of the MODIS and Landsat WSI maps for the snowy areas was also presented with error distribution patterns. The baseline snow cover led to the coefficient of determination values of 0.77 with the MODIS data and 0.78 with the Landsat data. The results indicated that Landsat images offered a suitable spatial resolution for the snow cover mapping using the WSI approach in regional studies. A finer resolution mapping of snow cover with the Landsat data can provide essential insights into the spatiotemporal dynamics at the local and regional scales.

1 Introduction

Snow cover plays a vital role in runoff and groundwater recharge patterns in mountainous regions (Akyürek and Şorman 2002; Jain et al. 2008). Variations in the cryosphere and climatic changes are most likely to exert significant effects on the regional distribution of snow cover. Accurate mapping of the snow cover dynamics can provide strategical insights into local and regional water management practices. In particular, monitoring of the snow cover in the Mediterranean region of Turkey is of high priority due to rapid

irregularities experienced in snow cover during the past decades. These irregularities may lead to the degradation and destruction of local hotspot ecosystems, such as rivers, and irrigated agriculture, thus, regional food insecurity.

Snow cover measurements are mostly done manually (Pirazzini et al. 2016). These measurements are extremely labor intensive, expensive, and dangerous under the complex topographical conditions. The use of telemetering of snow pillow and storage gauge measurements of precipitation has contributed to reducing the need for field campaigns. Still, it has not overcome the issue of the point-based measurements (Grossi et al. 2017). Uncertainties associated with the interpolation applications may cause an inaccurate representation of the snow potential of a given watershed (Grossi et al. 2017). Stewart (2009) detected that a warmer temperature affected snowpack at mid-elevations and resulted in an earlier meltdown. Hall et al. (2015) found that the increases in night air temperature during spring and summer led to earlier melting based on Landsat and MODIS data (1972–2013).

Remote sensing plays a crucial role in snow management by allowing for the ability to quantify the snow cover distribution in inaccessible areas (Haefner et al. 1997).

✉ Cenk Donmez
  cdonmez@cu.edu.tr

1 Landscape Architecture Department, Remote Sensing and GIS Lab., Cukurova University, Adana 01330, Turkey

2 Faculty of Engineering, Geomatics Engineering Department, Cukurova University, Adana, Turkey

3 Finnish Meteorological Institute, Erik Palmenin aukio 1, room 2A18a, 00560 Helsinki, Finland

Monitoring of snow cover in such regions is one of the crucial aspects of sustainable water management, where changes in the regional snow cover are required. Utilizing multiple end members in spectral mixture analysis (Rosenthal and Dozier 1996; Vikhamar and Solberg 2003; Salomonson and Appel 2004; Painter et al. 2009; Shreve et al. 2009) with a combination of multiple spectral bands is the most common remote sensing technique used to extract snow cover (Crane and Anderson 1984; Dozier 1989). Dietz et al. (2012) provided a detailed review of the remote sensing techniques for snow cover. They reviewed the discrete methods for the identification of snow cover with optical sensors. They found out the threshold value of Normalized Difference Snow Index (NDSI) > 0.4 was used to indicate snow coverage to map snow extent automatically with NDSI. This value has been suggested by Hall et al. (1995) after extensive analyses, and Klein and Barnett (2003) proved that an NDSI value > 0.4 indicates snow-covered surfaces. The NDSI threshold can be decreased to prevent underestimation because forests tend to mask out the snow-covered ground. Fractional Snow Cover (FSC) is one of the most readily identifiable measures derived from aerial photography or satellite imagery to secure water resources (Nolin 2011). Metsämäki et al. (2018) used FSC data to create maps of snow melt-off days and detected a decrease in melt day.

NDSI is produced from the normalized difference between green (RG) and shortwave infrared (RS) band reflectance to map snow cover, in particular, with the help of Moderate Resolution Imaging Spectroradiometer (MODIS) data (Hall et al. 2002; Hall and Riggs 2007). The studies found that the MODIS binary snow cover products have a good fit with both in situ measurements and the satellite-based snow cover products (Klein and Barnett 2003; Maurer et al. 2003; Parajka and Blöschl 2008). Rosenthal and Dozier (1996) mapped FSC using a decision tree-based classification model based on the Landsat TM data. Pepe et al. (2005) explored Envisat, Medium Resolution Imaging Spectrometer (MERIS) and Advanced Along Track Scanning Radiometer (AATSR) platforms to monitor the snow cover in Alpine regions. Sharma et al. (2016) developed a Water-Resistant Snow Index (WSI) as one of the cutting-edge approaches in the binary snow mapping. WSI includes an efficient algorithm to extract the snow cover. It does not interfere with ground objects and water surfaces. WSI exploits a hue, saturation, and value (HSV) color model (Smith 2011), where H indicates a perceived color of the spectral property such as red, yellow, and green, while V and S show the color and gray brightness.

In contrary to the MODIS data (Justice and Townshend 2002; Sharma et al. 2016), an explicit representation of the finer spatial variability of snow cover is essential to make an accurate simulation of hydrological conditions. Thus far, the researchers have mostly applied snow indices using coarser resolution data. Therefore, there is a need to explore to detect the snow cover with finer resolution snow indices. In so doing, Landsat data, which have a 30-m spatial resolution, may be leveraged to resolve the snow cover patterns across complex terrains. Ground truth data from the snow stations were used as the validation data to produce reliable WSI data (Sharma et al. 2016). For example, Piazzi et al. (2019) assessed the potential of the Sentinel-2A products to determine the accuracy of the moderate-resolution snow cover products. They found close agreement between the Sentinel-2A data and ground observations.

In this study, the applicability of WSI using MODIS and Landsat TM and OLI images was compared in the quantification of the snow cover at a complex catchment in the Eastern Mediterranean region of Turkey. The efficiency of the WSI solely based on multispectral imagery for robust detection, extraction, and mapping of snow cover at a regional scale was explored. Consecutive processing steps were applied to the shortwave infrared and visible Landsat spectral wavebands to derive the snow cover clearly with the WSI. The outputs comprised stand-alone maps of snow cover at watershed scale with no requirement for an external water mask.
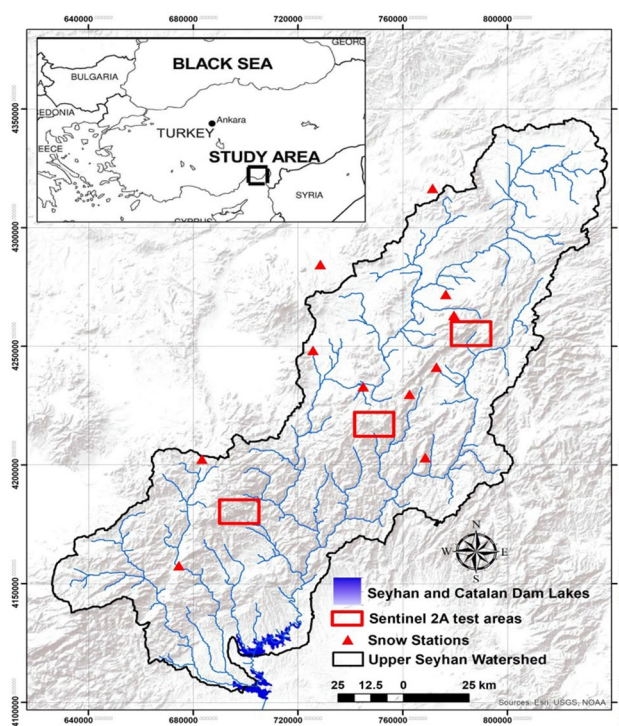

Fig. 1 Location of Upper-Seyhan Basin and existing snow stations

2 Materials and methods

2.1 Study area

The Seyhan watershed (18.900 km^2) (Fig. 1) selected for this study is located in the Eastern Mediterranean region of Turkey. The Eastern Mediterranean region is particularly vulnerable to potential changes in the snow cover due to its complex topography and heterogeneous landscape. It is also an important agricultural region (about 10% of the total irrigated agricultural production) in Turkey (Donmez and Berberoglu 2016). There are seven hydropower reservoirs located in the region, which directly affects the seasonal flow dynamics. Therefore, the sustainable management of its water resources is essential to sustainable agricultural production, ecosystem productivity, food security, and biodiversity of the region (Donmez et al. 2016).

The snow cover influences seasonal freshwater supplies and upstream–downstream linkages in the basin. Approximately 50% of the Upper Seyhan Basin is covered by snow in the winter months where snow melts between March and June with the temperature rise (Donmez et al. 2015). The snow cover provides a significant source of freshwater, which constitutes an important testbed for FSC to estimate through the recent remote sensing techniques accurately.

2.2 Data

Six Landsat TM, eight Landsat OLI, six MODIS Terra MOD09A1, and one Sentinel-2A cloud-free images were obtained in this study. These images were selected to represent the snow accumulation and ablation periods of the region. Table 1 lists the selected images.

Landsat 5 mission has a repeated coverage every 16 days in a sun-synchronous orbit and produces 185-km wide

Table 1 List of the selected remotely sensed images used in the study

Sensor	Date	Path/row
Landsat 5 TM	10 November 2005	175/34–175/36
	14 February 2006	175/34–175/36
	19 April 2006	175/34–175/36
Landsat 8 LDCM OLI/TIRS	27 November 2017	175/34–175/36
	15 February 2018	175/34–175/36
	4 April 2018	175/34–175/36
MODIS Terra MOD09A1	9 November 2005	
	18 February 2006	
	15 April 2006	
	25 November 2017	
	10 February 2018	
	7 April 2018	
Sentinel-2A	6 April 2018	

imagery at a 30-m ground resolution with the Worldwide Reference System (WRS). TM sensor scenes have seven spectral bands with a spectral range of 0.45–12.50 μm. LANDSAT 8 Operational Land Imager (OLI) images consist of nine spectral bands. Panchromatic band (band 8) has a 15-m spatial resolution as well as a 170 km north–south by 183 km east–west scene size. The MODIS/Terra-MOD09A1 images used in this study were the 8-day gridded level-3 products at a 500-m spatial resolution. The Landsat TM and OLI and MODIS images used in this study were derived from the United States Geological Survey (USGS) via Global Visualization Viewer (GloVis) free of charge (George 2018). The other data utilized in this study included the observed snow data and relief information. The relief information was derived from a Digital Elevation Model (DEM).

The satellite images and snow measurements were used as the reference dataset to validate the WSI maps. Two Sentinel-2A scenes acquired on 6 April 2018 at 10-m resolution were utilized as the testing data in this study due to its high temporal and spatial resolutions. These images were combined to cover the entire study area. The Sentinel-2A was successfully launched on 23 June 2015 to support generic land cover, land use, and change detection maps. In its standard band settings, there are 13 spectral bands (0.443–2.190 nm), from the near to the shortwave infrared at different spatial resolutions (ESA 2019). Sentinel-2A images used in this study were provided by the European Space Agency (ESA) within the Copernicus program. The snow measurements were obtained from available stations operated by State Hydraulic Works of Turkey (DSI). In the study region, there were 13 gauging and five snow stations in operation. These stations have recorded data irregularly from 2005 to 2018. Available ground data were obtained daily during 1985–2018 and used in the validation of the FSC maps produced in this study.

2.3 Methodology

Consecutive processing steps were required to apply the comprehensive comparison of MODIS and Landsat WSI outputs. Figure 2 displays the flow diagram of this study.

The first step was data processing, which included the geometric and radiometric corrections of the remotely sensed images. The relationship between input radiance and output digital number (DN) was tested and calibrated using a linear combination of the values of the corresponding pixels across the stack. After data processing, the MODIS and Landsat WSI maps were derived. These maps were then validated by incorporating the reference dataset derived from both the snow measurements and Sentinel-2A images. The potential of the Landsat WSI maps was then evaluated in terms of their availability for local studies.
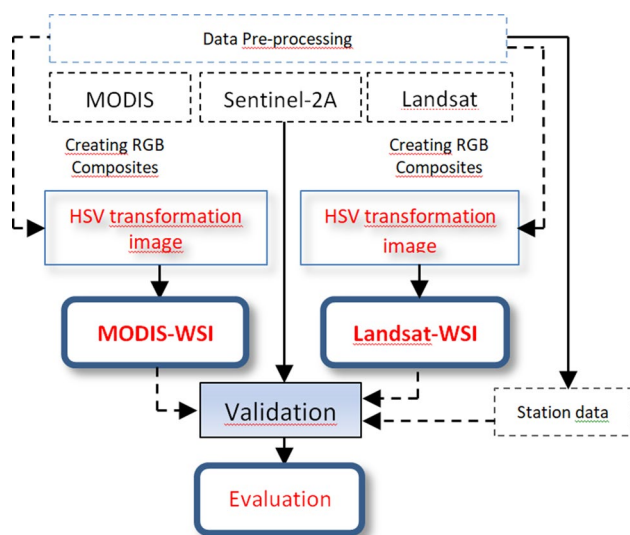
Fig. 2 Flow diagram of the study

2.4 Data pre-processing

A pre-processing step should be done before the image dataset can be used. Both Landsat 5 TM and OLI images were converted into the image format, and the bands were stacked for each image. They were projected into Universal Transverse Mercator (UTM) Zone 36 with World Geodetic System 1984 (WGS84) datum. Using the DEM data, a subset boundary was defined for the Seyhan Watershed, where the images were extracted accordingly to reduce the computing load and allow the most accurate comparison between the reference points and the images. Radiometric calibration was also performed for the Landsat images to reduce their noise level.

MODIS images were derived from the USGS in the sinusoidal projection system at 500 m. These images were geometrically corrected and projected to the WGS84 ellipsoid UTM system. Sentinel-2A images were derived from the ESA Copernicus Data Hub at 10 m (ESA 2019). These scenes were then combined to cover the study area and recorded to WGS 84 ellipsoid UTM projection system also. Sentinel-2A images were combined to cover the study region and subset to three sub-scenes as the testing areas from the different parts of the study area.

2.5 Deriving the WSI maps

Deriving the WSI snow maps using the MODIS and Landsat images was the core part of this study. Snow has relatively high reflectance in the visible part of the spectrum and shortwave regions than the other land types, such as water, soil, and vegetation (Warren 1982). In this study, the RGB color composites [red (RR), green (RG), and near-infrared (RN) reflectances] were converted into the color space of HSV for deriving the

MODIS and Landsat WSI maps. Then, the values (V) and H were defined from the HSV data as follows:

$$\mathrm{WSI} = \frac{V_{(R_R R_G R_N)} - H_{(R_R R_G R_N)}}{V_{(R_R R_G R_N)} + H_{(R_R R_G R_N)}}. \tag{1}$$

Within WSI, it is expected to distinguish a better snow cover discrimination from the other objects by differentiating the brightness (V) and spectral color (H) of the objects (Sharma et al. 2016). Discriminating the other objects from snow is possible since the snow-covered areas are brighter at all the red, green, and near-infrared wavelengths.

At first, value (V), hue (H), and their normalized difference were calculated. Then the WSI for MODIS was developed to differentiate snow-covered areas and water bodies from the HSV data. After processing and mapping the MODIS WSI, the WSI method was applied to both Landsat 5 TM and OLI images to derive the WSI maps at a 30-m resolution. The difference between V and H was standardized between -1 and 1 for both MODIS and Landsat data. The WSI values were recorded as eight-bit unsigned integers. Their dynamic range was scaled between 0 and 255 to facilitate further image processing (Sharma et al. 2016).

2.6 Validation and comparative analysis

Validation is a challenging task but compulsory to provide reliable snow cover outputs. In this study, the validation of the MODIS and Landsat WSI maps over the study region was performed by utilizing the snow measurements and also Sentinel-2A images to assess the accuracy of the WSI maps, statistically.

Snow depth obtained from the meteorological stations was utilized as a reference point closest to each station. These pixels were taken into account as the snow cover when the observed snow depth exceeded 0.1 cm and as snow free otherwise. The location of these snow stations was overlaid with the modified WSI maps, and thus, snow cover information was extracted.

Due to the limited number of snow observations available in some areas of the region, Sentinel-2A data with a 10-m spatial resolution were also utilized to enhance the reference dataset for validation because of its spectral and high spatial resolution. Three sub-scenes of Sentinel-2A images representing the different parts of the study area were used to derive the baseline data of the snow cover. Using Sentinel 2A subsets, snow cover was classified and recoded as snow versus non-snow pixels at a 10-m spatial resolution. One hundred fifty points were randomly selected for each sub-scene. The snow cover information was extracted from the Sentinel 2-A classification through these points.

A regression was applied to the output maps and testing dataset, including snow measurements and Sentinel-2A, to examine the performance of Landsat data in the WSI derivation. The cross-validation based on a Nagelkerke regression (r^2_{NAG}) was employed to the MODIS and Landsat WSI data against snow information from both snow stations and Sentinel 2-A snow cover. r^2_{NAG} was based on the Cox and Snell model (Haigh et al. 1990) using the following equation (Nagelkerke 1991):

$$r^2_{\mathrm{NAG}} = 1 - \exp\left[2\left(n^{-1}\right)L(0)\right] = 1 - L(0)^{\frac{2}{n}}. \tag{2}$$

It compared to the log-likelihood of a baseline model, then based on the log-likelihood for the model where n is the sample size. r^2_{NAG} varied between 0 and 1, with positive values indicating a better correlation between the variables. For a comparative analysis, a regression model was applied to the MODIS and Landsat WSI maps to plot their pixel-based error distributions.

3 Results

The study aimed to compare the applicability of WSI with Landsat images to explore the potential improvement of its spatial variability in quantifying the FSC at a better spatial resolution. The applicability of WSI for the snow cover mapping was tested using Landsat TM and OLI in a complex catchment located in the Eastern Mediterranean region of Turkey. The cloud-free images were selected to represent the snow accumulation, snowpack, and ablation periods for obtaining the distribution of snow cover over the entire watershed. Near date images were used for the change detection analysis. The radiometric correction was also performed to make an effective and accurate comparison by preventing the spectral mixing in the images. To extract the snow cover information, WSI was applied utilizing the near-IR and RGB bands of the MODIS and Landsat TM/OLI datasets. RGB color composites were constituted and transformed into the HSV color model.

To test the reliability of the WSI maps, a validation procedure was accomplished. Ground measurements derived from the 13 available snow stations in the study area were incorporated with the WSI maps as well as the Sentinel-2A sub-scenes. The WSI maps derived from MODIS and the Landsat images showed a good agreement with 0.77 and 0.78 r^2_{NAG}, respectively, (Nagelkerke regression). The overall accuracy r^2_{NAG} indicated close agreement between the WSI maps and the ground snow observations.

The accuracy of the spatially distributed WSI maps was defined through validation against the reference data. The Sentinel-2A test sub-scenes, each covering 150 km^2, were classified to be used also as the ground truth data. The snow classification results were then generalized to estimate the snow cover at the MODIS and Landsat-based spatial resolutions using the nearest neighbor technique. RGB formats of the Sentinel-2A sub-scenes, and their classified and generalized versions are given in Fig. 3.

The coverage of the Sentinel-2A dataset was equal to 167,334 Landsat OLI pixels and 943 MODIS Terra MOD09A1 pixels. Within these validation periods, both WSI maps derived from the MODIS and Landsat sets were evaluated using the r^2_{NAG} values on a particular day. The overall accuracy r^2_{NAG} of about 0.85 for MODIS and 0.87 for Landsat pointed to close agreement between the WSI maps and the spatially generalized test data derived from Sentinel-2A.

The misclassification errors showed that the most remarkable errors occurred in February, while this was the month with the largest snow cover. Also, the errors were smaller in winter and when there was a well-developed snowpack in autumn. The validated WSI maps derived from the MODIS/Terra-MOD09A1 and Landsat TM/OLI data are given in Figs. 4 and 5, respectively. The DEM data were used to generate the watershed boundary, and thus, the output images.

Figure 6 shows the validated NDSI maps derived from the MODIS/Terra-MOD09A1 set.

The Landsat 5 TM WSI maps in February showed the well-developed snowpack covering the whole northern region of the watershed. The mean altitude of the snow-covered areas is 1400 m. In November, snow was presented only in the uplands at the highest elevations in 2005 and 2017. A spectacular snow difference occurred from 2009 to 2017 in the region for February within a high snowpack difference. Also, a decrease in snow occurred in the northern areas of the region and partly in the Central Anatolia with the terrestrial climate characteristics. In April, an increase in the snow was detected slightly more than its decrease when snow existed only on the highlands over 1000 m. Table 2 includes the snow cover derived from the MODIS and Landsat WSI maps.

Table 3 presents the calculated snow area from the NDSI maps of MODIS images.

Based on both MODIS and Landsat WSI maps, dramatic snow changes occurred in the Seyhan watershed over 12 years. The most considerable change was observed between February 2006 and 2018. The extent of snow cover in the study region varied with each term defined in this study. During the prediction period of 12 years, a negative difference of 700,000 ha was detected for February. These results indicated that a seasonal shift occurred; in other words, the timing of the accumulation and ablation periods started to change in the last 12 years. The increased snow in April also confirmed this shift and indicated a more extended melting season, which ended in the early summer. The extended melting season may cause unanticipated loads
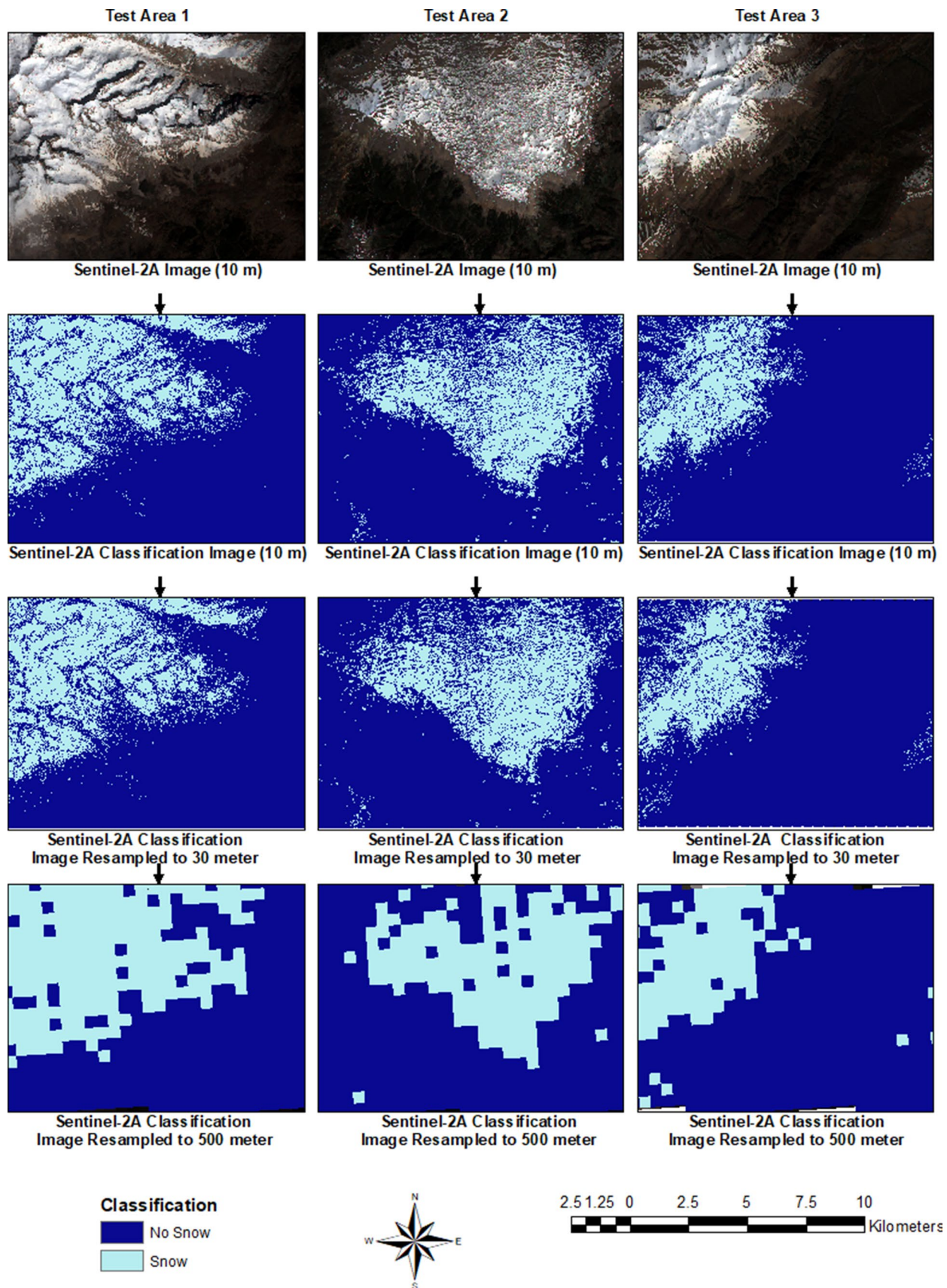
Test Area 1 **Test Area 2** **Test Area 3**

Sentinel-2A Image (10 m) Sentinel-2A Image (10 m) Sentinel-2A Image (10 m)

Sentinel-2A Classification Image (10 m) Sentinel-2A Classification Image (10 m) Sentinel-2A Classification Image (10 m)

Sentinel-2A Classification Image Resampled to 30 meter Sentinel-2A Classification Image Resampled to 30 meter Sentinel-2A Classification Image Resampled to 30 meter

Sentinel-2A Classification Image Resampled to 500 meter Sentinel-2A Classification Image Resampled to 500 meter Sentinel-2A Classification Image Resampled to 500 meter

Classification
- No Snow
- Snow

Fig. 3 RGB formats of the Sentinel-2A sub-scenes and their classified and generalized versions for test areas (1, 2, and 3)

Fig. 4 The WSI maps of the study region derived from MODIS/Terra-MOD09A1
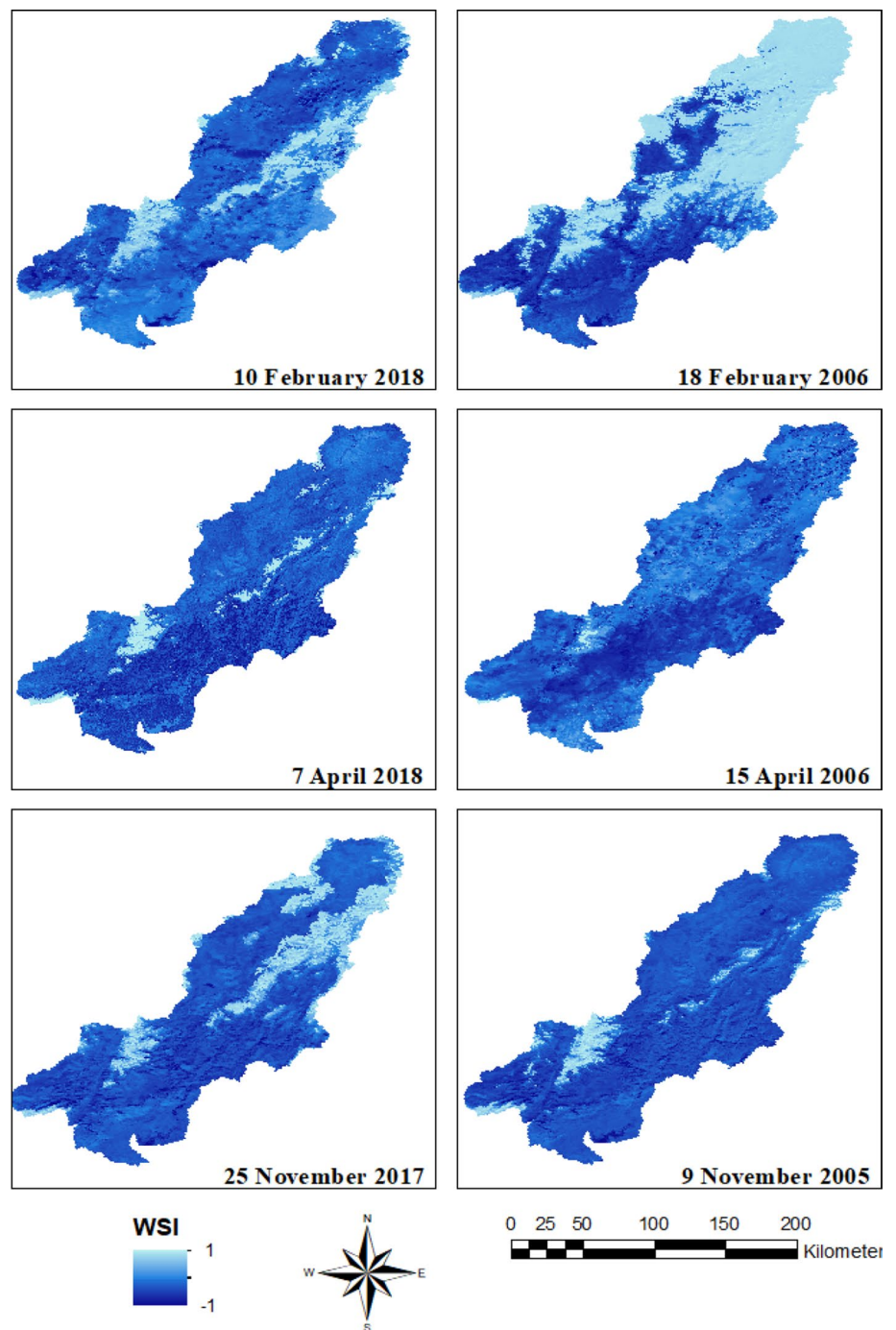
of water to the downstream areas in the summer seasons in the region where the hydropower reservoirs are located. For February, a considerable increase in the snow cover was detected and compared to the other months for both images. Also, April witnessed a total of 66,493 ha gain and 281 ha loss. These results showed that adaptation measures for varied snow melting should be taken to ensure better management scenarios, particularly for hydropower management, efficient irrigation, and flood risks. Overall, the difference maps indicated a significant variation in the snow cover.

These changes indicated a substantial amount of irregularity in precipitation, which led to a considerable change in the regional snow cover. The trends in the snow cover showed irregularities in their spatial distribution. For instance, the increase in February mostly occurred in the lowlands close to the main settlement areas (e.g., the Adana city). Only slight snow decreases were observed in the highlands in winter. The altitudinal ranges of the snow cover were between 50 and 3700 m approximately. The spring/early summer periods also showed slight increases in snow, which might

Fig. 5 The WSI maps of the
study region derived from
Landsat TM and OLI data
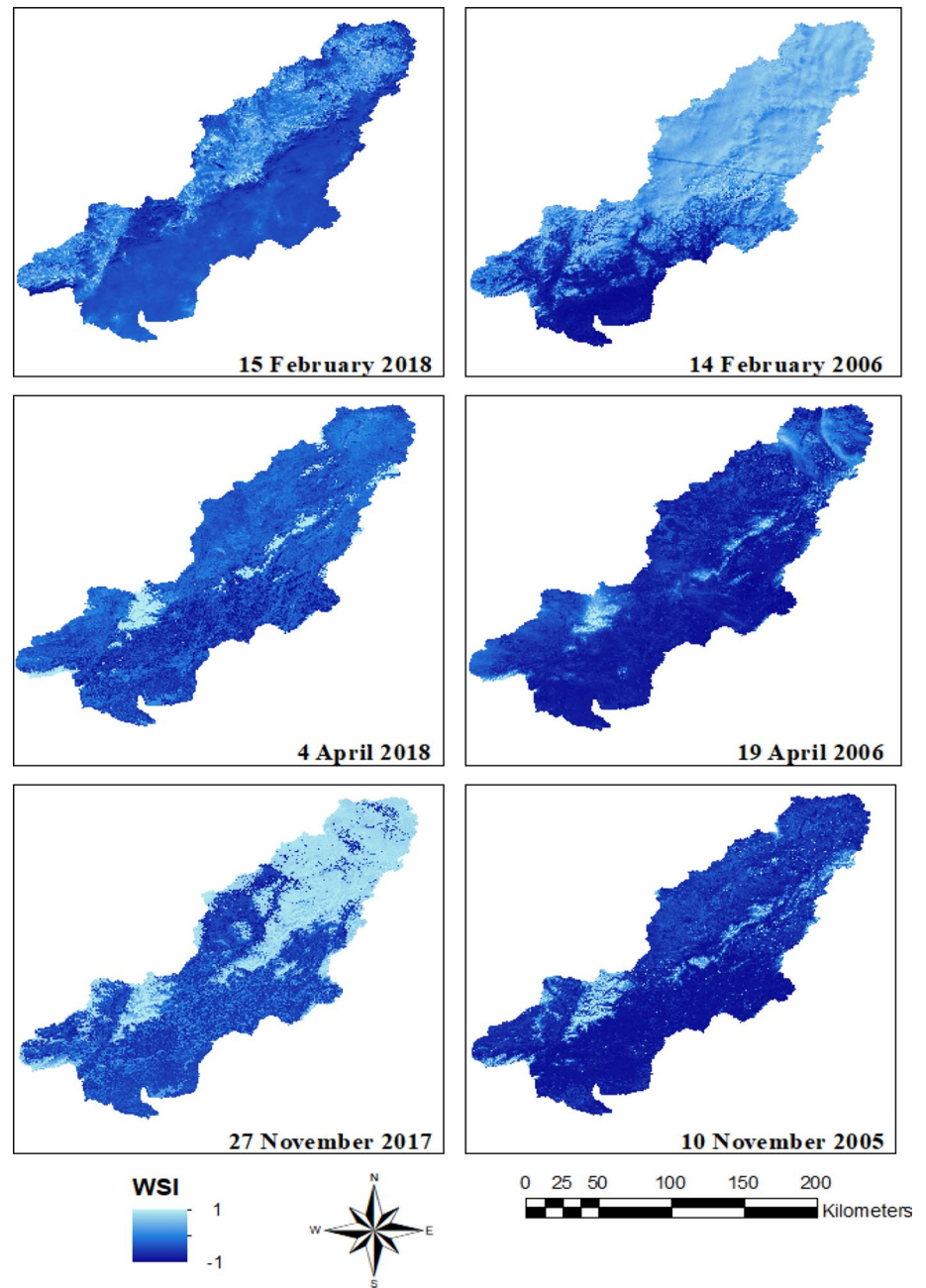
be an indication for an extension of the ablation period in the region. The remarkable differences among the difference maps can be referred to as the possible effects of climate change on the annual variation in the snow cover.

According to the WSI maps, the change in November mostly occurred in the upper watershed. The topographic structure of the river basin affects the climate differences that might significantly change the snow cover. The lowlands of the lower part of the watershed faced extensive urbanization and agricultural activities, with no significant change in these areas. The decrease in February was possibly due to the seasonal effect; however, the dramatic changes in November needed to be clarified. The comparative analysis of the MODIS and Landsat WSI maps for the snowy areas showed the snow cover distribution for the 3 months of February, April, and November. Figure 7 shows the histogram of the snow cover distributions significantly differed between the MODIS and Landsat WSI maps.

Fig. 6 The NDSI maps of the study region derived from MODIS/Terra-MOD09A1 data
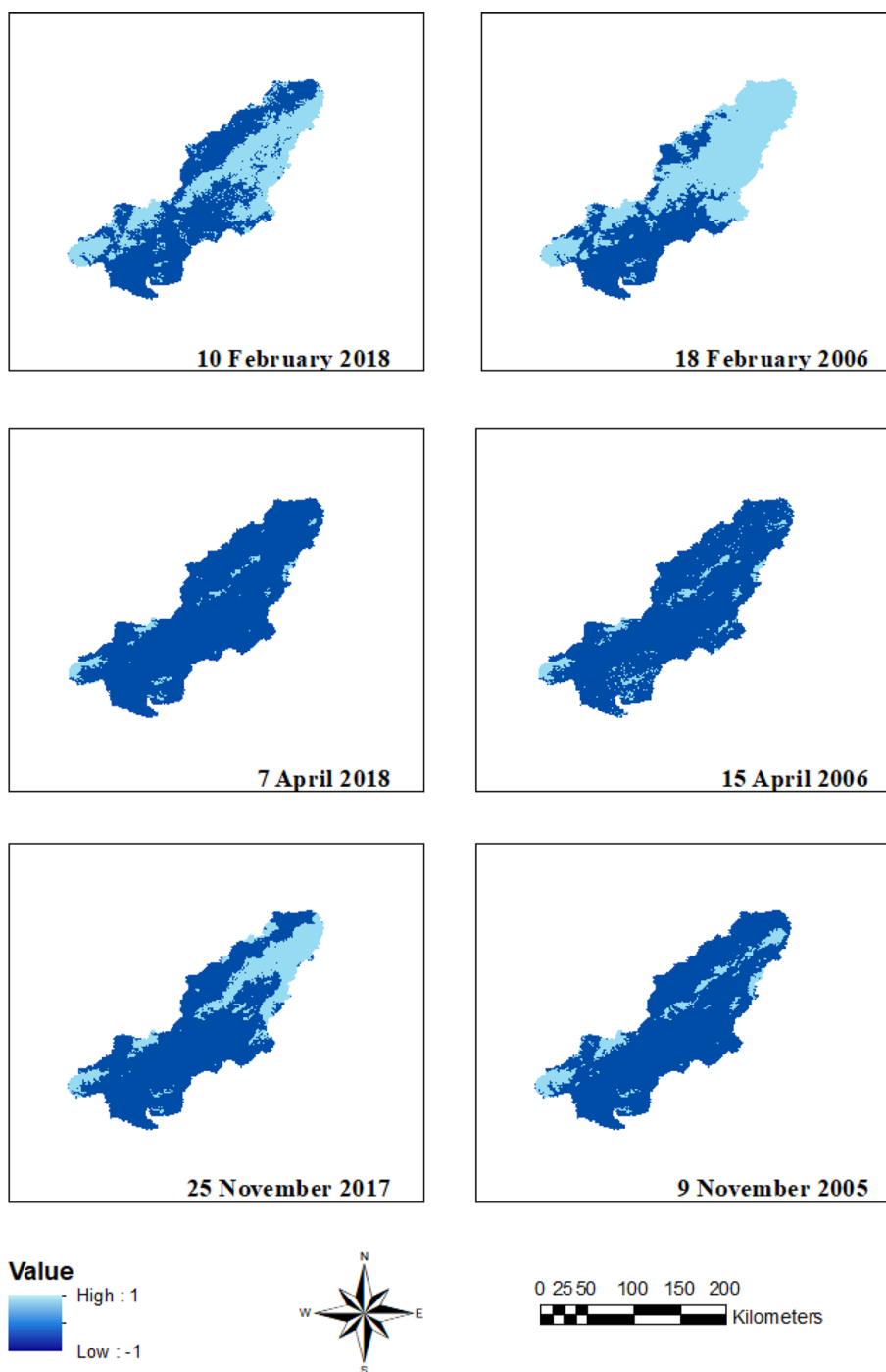
The error distribution patterns showed the distribution of the differences between the predictions and the reference data. The MODIS images showed prediction errors mostly throughout the snow cover. Compared to the Landsat imagery, the MODIS prediction error was evenly distributed. Generally, the largest error for the snow cover was found in the lower regions of the MODIS WSI predictions. The quantity and spatial distribution of snow are highly affected by elevation. Figure 8 shows the comparative analysis of the MODIS and Landsat WSI in the different altitudes.

A strong variability of the snow cover was attributed to the weather conditions and the local relief interactions in the range of 200–3700 m in the study area. The changes in the

Table 2 Snow cover extent information derived from the MODIS and Landsat WSI maps

Data range	MODIS		Landsat	
	WSI pixels	Area (ha)	WSI pixels	Area (ha)
November 2005	4734	118,350	1,500,371	135,033
February 2006	40,549	1,013,725	11,524,800	1,037,232
April 2006	1303	32,575	569,572	51,261
November 2017	11,463	286,575	1,120,891	100,880
February 2018	13,035	325,875	3,517,757	316,598
April 2018	1274	31,850	454,171	40,875

Table 3 Snow cover extent information derived from the MODIS NDSI maps

Data range	MODIS	
	NDSI pixels	Area (ha)
November 2005	9587	239,675
February 2006	50,278	1,256,950
April 2006	6742	168,550
November 2017	21,382	534,550
February 2018	34,393	859,825
April 2018	3914	97,850

snow cover were investigated, incorporating the DEM and snow change images. The regional topographical characteristics were linked to the snow difference areas to assess the changes in the snow cover in the different altitudes. Only the snow change pixels were taken into account, and thus, the gain/loss values were linked to the elevation pixels. Once the snow change pixels with 0 values were removed, the elevation versus the snow change pixel values was plotted.

The combination of WSI and DEM enabled the areas where the changes in the snow cover started and ended to be detected. The highest snow changes were detected in November at 3613 m for the entire period. A level of 1615 m was identified in February and 2422 m in April as the mean elevation of the increased snow in the study area. The snow covers in the higher altitudes showed a remarkable increase in November. In particular, the increased spatial distribution of snow as was detected with these months indicated a possible shift of the regional climate characteristics from the Central Anatolia to the Mediterranean region of Turkey.

4 Conclusions

The snow cover information is crucial for the sustainable management of water resources, particularly in the Mediterranean regions, where water scarcity is exacerbated by climate change. Remote sensing offers the ability to quantify the spatiotemporal dynamics of snow in complex terrains where such measurements are impossible or very limited for the monitoring and mapping of snow cover with finer resolution. The superiority of WSI over NDSI has been proven in many case studies about snow-covered regions. However, WSI has only been trained and applied with MODIS data. Thus, this study explored the potential improvement of the spatial variability of WSI using Landsat images in the quantification of the snow cover fraction at a better spatial resolution in the Eastern Mediterranean region of Turkey. The shortwave infrared and visible Landsat spectral wavebands used to derive the snow cover clearly showed the enhancement of the NDSI and WSI snow indices. Landsat images offered a suitable spatial resolution for the snow cover mapping. They produced the snow cover maps with reasonable accuracy for the regional studies based on the WSI approach. However, the Landsat images still have a remarkable disadvantage to monitor the snow changes periodically due to their limited cloud-free availability. A significant variation in the snow cover was found to exist, which did not follow a linear trend for the different periods. The large differences among the snow cover maps may relate to the possible effects of climate change on the annual snow cover variation. There is a need to quantify the impacts of climate change on the regional snow dynamics through the integration of process-based snow modeling, remote sensing, and in situ data. The overall validation accuracy of 77% was obtained for both MODIS and Landsat images. Sentinel-2A data with the finer resolution were also used in the accuracy assessment of the snow maps. The Landsat data were slightly more accurate than MODIS data for the WSI-derived snow cover estimations. The WSI also allowed mapping the snow in topographically variable parts of the region where there was an inconsistent shadow effect. The DEM integrated WSI maps revealed the snow distributions in the different altitudes. However, the MODIS data are still more advantageous than the Landsat data in the periodical snow monitoring and mapping over the large regions owing to their frequent and composite image availability.
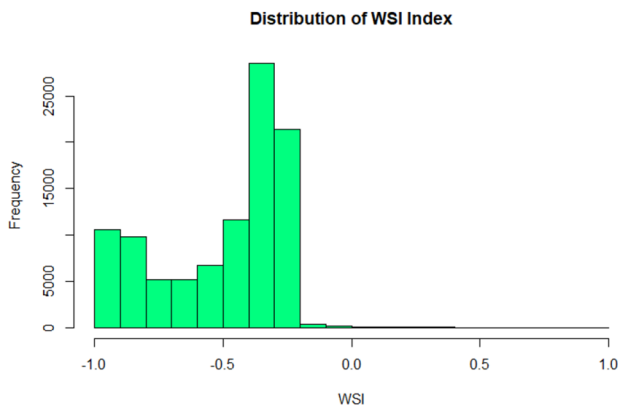
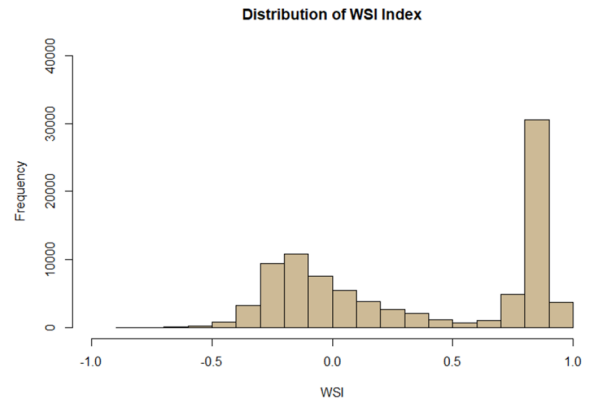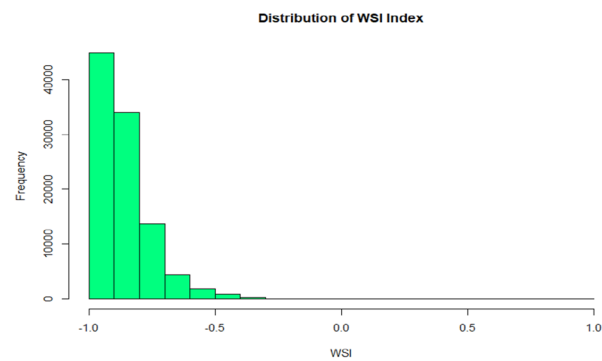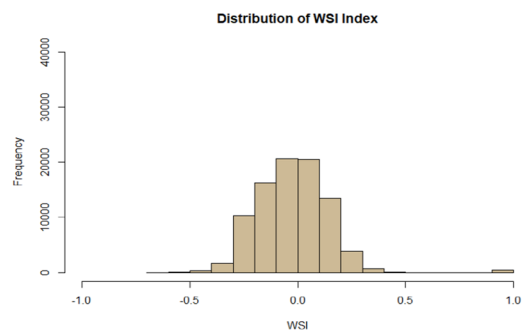Landsat TM/OLI

MODIS/Terra-MOD09A1
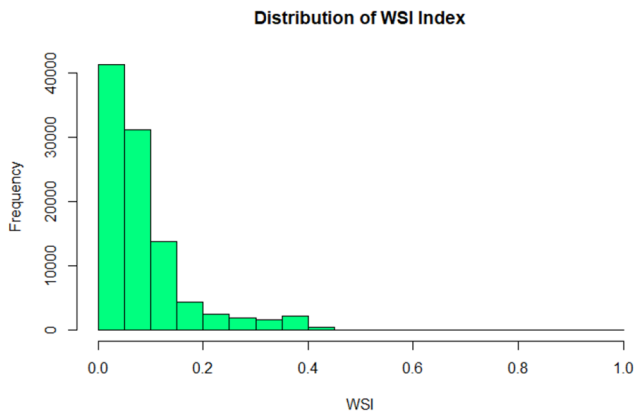
10 November 2005
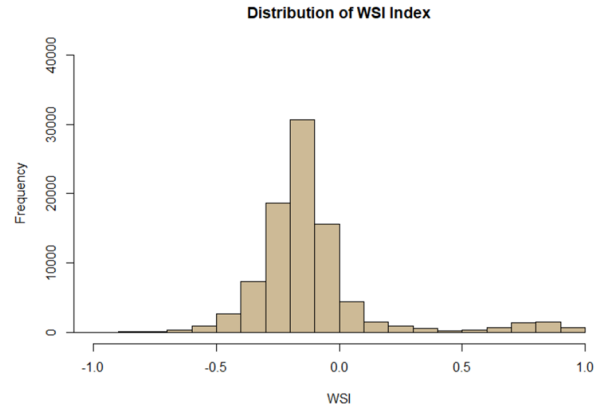
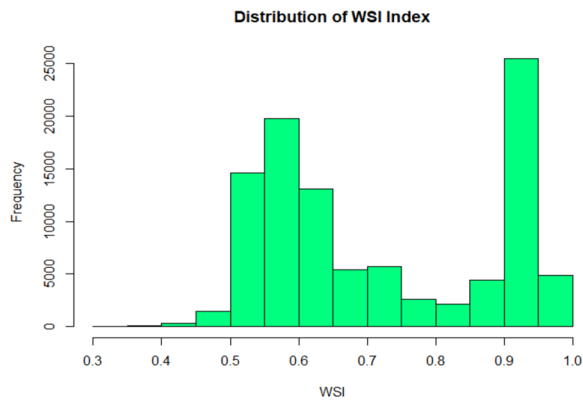9 November 2005

15 February 2006

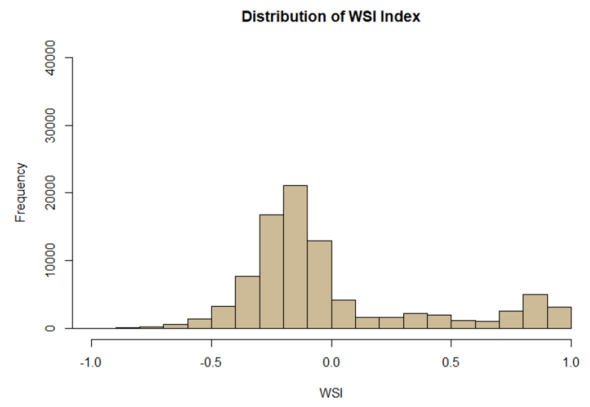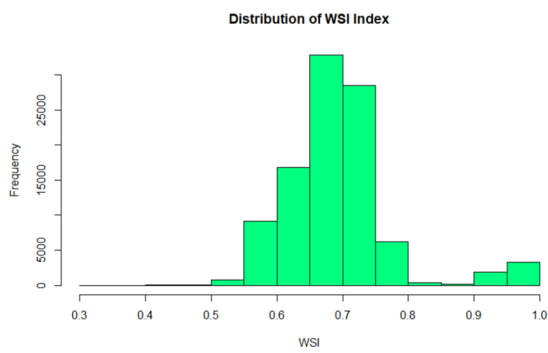18 February 2006

19 April 2006

15 April 2006

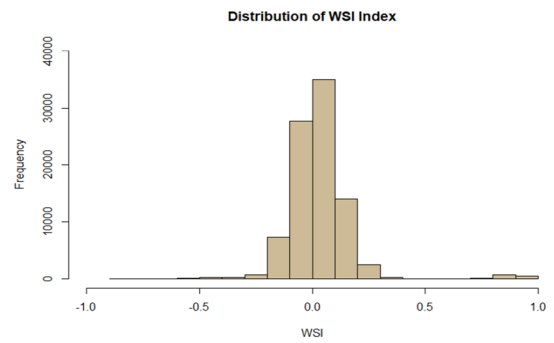**Fig. 7** The histogram of the snow cover distribution significantly differed for MODIS and Landsat

27 November 2017

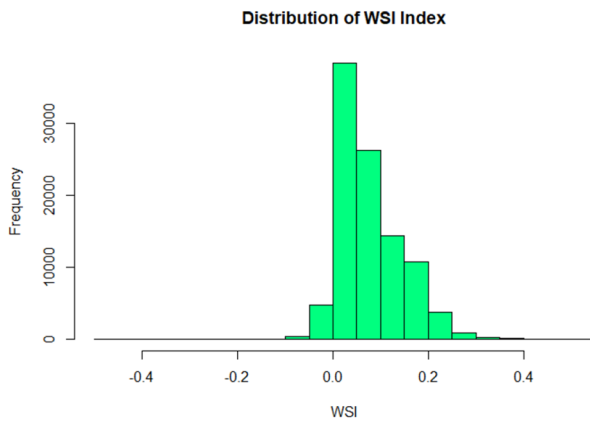**25 November 2017**

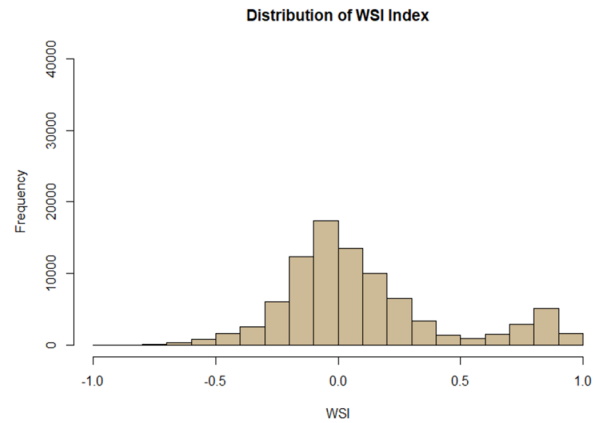**4 April 2018**

7 April 2018

15 February 2018

10 February 2018

Fig. 7 (continued)
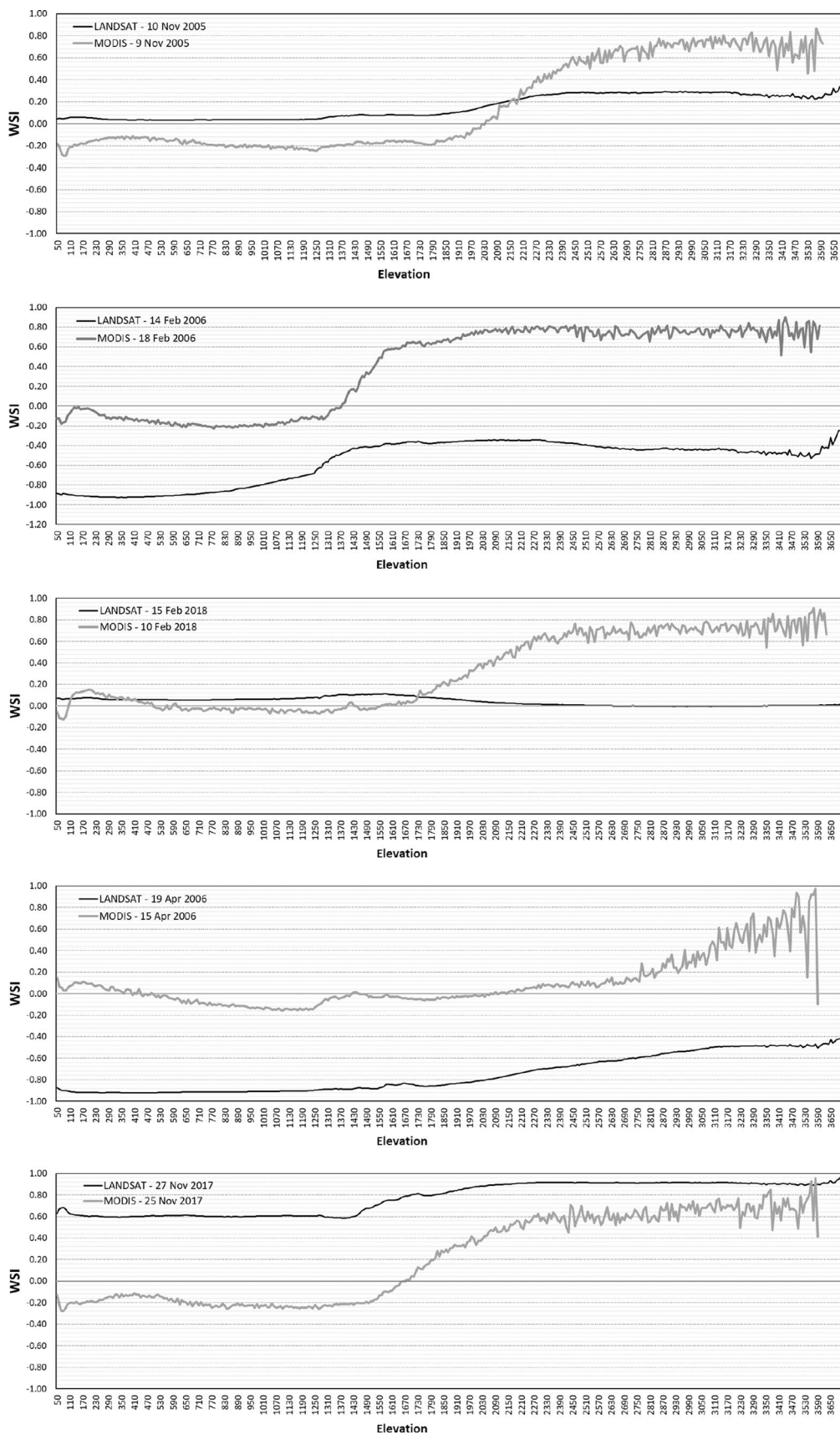
Fig. 8 Snow cover distribution patterns of the MODIS and Landsat WSI maps at different altitudes

References

Akyürek Z, Şorman A (2002) Monitoring snow-covered areas using NOAA-AVHRR data in the eastern part of Turkey. Hydrol Sci J 47:243–252

Crane RG, Anderson MR (1984) Satellite discrimination of snow/cloud surfaces. Int J Remote Sens 5:213–223

Dietz AJ, Kuenzer C, Gessner U, Dech S (2012) Remote sensing of snow—a review of available methods. Int J Remote Sens 33:4094–4134

Donmez C, Berberoglu S (2016) A comparative assessment of catchment runoff generation and forest productivity in a semi-arid environment. Int J Digit Earth 9:942–962. https://doi.org/10.1080/17538947.2016.1158875

Donmez C, Berberoglu S, Erdogan MA et al (2015) Response of the regression tree model to high-resolution remote sensing data for predicting percent tree cover in a Mediterranean ecosystem. Environ Monit Assess 187:4

Donmez C, Berberoglu S, Cilek A, Evrendilek F (2016) Spatiotemporal modeling of net primary productivity of Eastern Mediterranean biomes under different regional climate change scenarios. Int J Environ Res 10(2):341–356 **(ISSN: 1735-6865)**

Dozier J (1989) Spectral signature of alpine snow cover from the Landsat thematic mapper. Remote Sens Environ 28:9–22

ESA (2019) European Space Agency Data Hub. https://scihub.copernicus.eu/dhus/#/home

George MW (2018) United States Geological Survey. In: Miner. Commod. Summ. https://minerals.usgs.gov/minerals/pubs/commodity/mercury/myb1-2016-mercu.pdf

Grossi G, Lendvai A, Peretti G, Ranzi R (2017) Snow precipitation measured by gauges: systematic error estimation and data series correction in the central Italian Alps. Water 9:461

Haefner H, Seidel K, Ehrler H (1997) Applications of snow cover mapping in high mountain regions. Phys Chem Earth 22:275–278

Haigh J, Cox DR, Snell EJ (1990) Analysis of binary data, 2nd edn. Chapman and Hall, London

Hall DK, Riggs GA (2007) Accuracy assessment of the MODIS snow products. Hydrol Process 21:1534–1547. https://doi.org/10.1002/hyp.6715

Hall DK, Riggs GA, Salomonson VV (1995) Development of methods for mapping global snow cover using moderate resolution imaging spectroradiometer data. Remote Sens Environ 54:127–140

Hall DK, Riggs GA, Salomonson VV et al (2002) MODIS snow-cover products. Remote Sens Environ 83:181–194

Hall DK, Crawford CJ, DiGirolamo NE et al (2015) Detection of earlier snowmelt in the Wind River Range, Wyoming, using Landsat imagery, 1972–2013. Remote Sens Environ 162:45–54

Jain SK, Goswami A, Saraf AK (2008) Accuracy assessment of MODIS, NOAA, and IRS data in snow cover mapping under Himalayan conditions. Int J Remote Sens 29:5863–5878

Justice C, Townshend J (2002) Special issue on the moderate resolution imaging spectroradiometer (MODIS): a new generation of land surface monitoring. Remote Sens Environ 83:1–2

Klein AG, Barnett AC (2003) Validation of daily MODIS snow cover maps of the Upper Rio Grande River Basin for the 2000–2001 snow year. Remote Sens Environ 86:162–176

Maurer EP, Rhoads JD, Dubayah RO, Lettenmaier DP (2003) Evaluation of the snow-covered area data product from MODIS. Hydrol Process 17:59–71

Metsämäki S, Böttcher K, Pulliainen J et al (2018) The accuracy of snow melt-off day derived from optical and microwave radiometer data—a study for Europe. Remote Sens Environ 211:1–12

Nagelkerke NJD (1991) A note on a general definition of the coefficient of determination. Biometrika 78:691–692

Nolin AW (2011) Recent advances in remote sensing of seasonal snow. J Glaciol 56:1141–1150

Painter TH, Rittger K, McKenzie C et al (2009) Retrieval of subpixel snow-covered area, grain size, and albedo from MODIS. Remote Sens Environ 113:868–879

Parajka J, Blöschl G (2008) The value of MODIS snow cover data in validating and calibrating conceptual hydrologic models. J Hydrol 358:240–258

Pepe A, Sansosti E, Berardino P, Lanari R (2005) On the generation of ERS/ENVISAT DInSAR time-series via the SBAS technique. IEEE Geosci Remote Sens Lett 2:265–269

Piazzi G, Tanis C, Kuter S et al (2019) Cross-country assessment of H-SAF snow products by Sentinel-2 imagery validated against in-situ observations and webcam photography. Geosciences 9:129

Pirazzini R, Leppänen L, Picard G, Lopez-Moreno JI, Marty C, Macelloni G, Kontu A, Von Lerber A, Tanis CM, Schneebeli M, De Rosnay P, Arslan AN (2016) European in-situ snow measurements: practices and purposes. Sensors 2018:18

Rosenthal W, Dozier J (1996) Automated mapping of montane snow cover at subpixel resolution from the landsat thematic mapper. Water Resour Res 32:115–130

Salomonson V, Appel I (2004) Estimating fractional snow cover from MODIS using the normalized difference snow index. Remote Sens Environ 89:351–360

Sharma RC, Tateishi R, Hara K (2016) A new water-resistant snow index for the detection and mapping of snow cover on a global scale. Int J Remote Sens 37:2706–2723

Shreve CM, Okin GS, Painter TH (2009) Indices for estimating fractional snow cover in the Western Tibetan plateau. J Glaciol 55:737–745

Smith AR (2011) Transnational dimensions of cold war anticommunism: actions, networks, transfers. Color Gamut Transform Pairs 136:23–42

Stewart IT (2009) Changes in snowpack and snowmelt runoff for key mountain regions. Hydrol Process 23:78–94

Vikhamar D, Solberg R (2003) Subpixel mapping of snow cover in forests by optical remote sensing. Remote Sens Environ 84:69–82

Warren SG (1982) Optical properties of snow. Rev Geophys 20:67–89

Publisher's Note Springer Nature remains neutral with regard to jurisdictional claims in published maps and institutional affiliations.